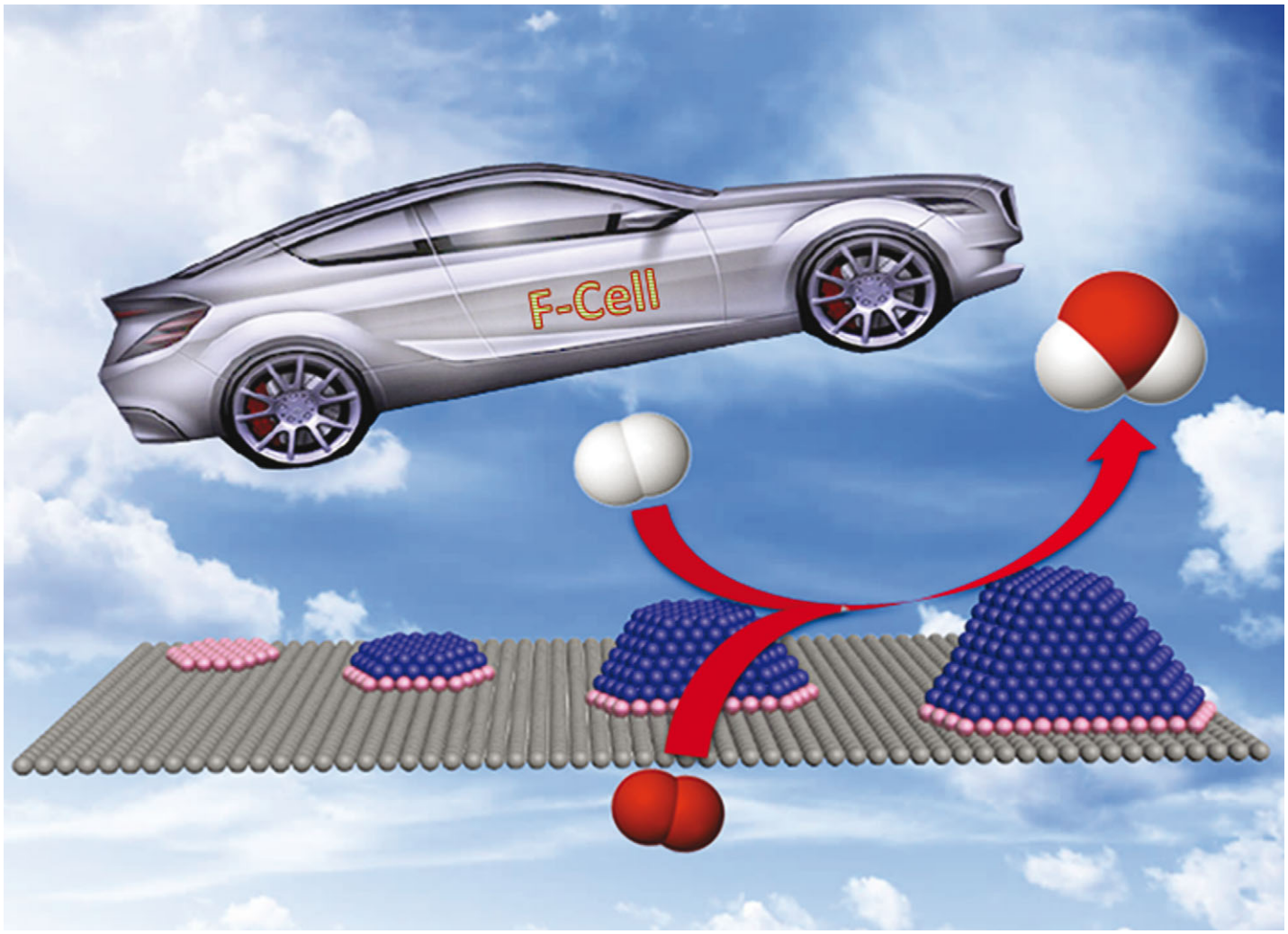

Showcasing research from Prof. Xueliang (Andy) Sun's group at The University of Western Ontario, Canada

Atomic scale enhancement of metal–support interactions between Pt and ZrC for highly stable electrocatalysts

Fuel cells are a promising solution for clean energy technology, but the instability of platinum (Pt) is a considerable challenge for its widespread adoption. Here, we used the advanced atomic layer deposition (ALD) technique to stabilize Pt catalysts by increasing the Pt–support interactions through precisely controlling the metal–support interface at the atomic level.

As featured in:

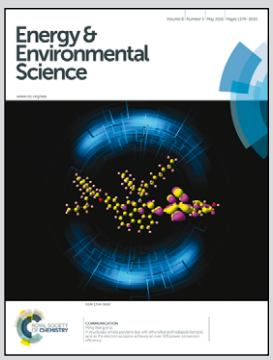

See Xueliang Sun *et al.*, *Energy Environ. Sci.*, 2015, **8**, 1450.

ROYAL SOCIETY OF CHEMISTRY

www.rsc.org/ees

Registered charity number: 207890

Energy & Environmental Science

COMMUNICATION

View Article Online
View Journal | View Issue

Cite this: *Energy Environ. Sci.*, 2015, **8**, 1450

Received 28th December 2014,
Accepted 5th February 2015

DOI: 10.1039/c4ee04086d

www.rsc.org/ees

Atomic scale enhancement of metal–support interactions between Pt and ZrC for highly stable electrocatalysts†

Niancai Cheng,[a] Mohammad Norouzi Banis,[a] Jian Liu,[a] Adam Riese,[a] Shichun Mu,[b] Ruying Li,[a] Tsun-Kong Sham[c] and Xueliang Sun*[a]

To further obtain high catalytic activity and durability of Pt catalysts for oxygen reduction reaction (ORR), we synthesized a robust Pt-on-ZrC nanocomposite catalyst by taking advantage of atomic layer deposition (ALD) to improve the strong metal–support interactions at the atomic level. X-ray absorption near edge structures (XANES) results show that ALD-Pt/ZrC catalysts show noticeable change in the electronic structure of Pt due to strong interactions with the ZrC support. Using electrochemical cycling to test durability, we found the ALD-Pt/ZrC nanocomposites to be roughly 5-fold and 3-fold more stable than commercial Pt/C and CW-Pt/ZrC (synthesized by a conventional chemical reduction method), respectively. The ALD-Pt/ZrC nanocomposite showed a mass activity of 0.122 A mg_{Pt}^{-1} at 0.9 V (*vs.* RHE); much higher than those for Pt/C and CW-Pt/ZrC catalysts (0.074 and 0.041 A mg_{Pt}^{-1}, respectively). After durability test, our novel catalyst also exhibited ORR activity 9 times greater than Pt/C. This approach, using ALD to grow the Pt catalyst directly, resulting in strong interactions, will aid the design of new active and stable catalysts for ORR or other chemical reactions.

Broader context

Fuel cells are a promising solution for clean energy technology because they offers high energy conversion efficiency and low emission of pollutants. However, low activity and the instability of platinum (Pt) are considerable challenges for widespread adoption of proton exchange membrane fuel cells in practical applications. Moreover, the corrosion of carbon support and the weak interaction between Pt and support in the catalysts is one of the major factors affecting their stability. Herein, we used the advanced atomic layer deposition (ALD) technique to stabilize Pt catalysts by increasing the Pt-support interactions through precisely controlling the metal–support interface at the atomic level. More corrosion-resistant zirconium carbide (ZrC) was used as support for deposition of ALD Pt to promote Pt oxygen reduction reaction (ORR) activity. ALD-Pt/ZrC catalyst exhibited very high activity and durability towards ORR compared with CW-Pt/ZrC (synthesized by a conventional chemical reduction method) and commercial Pt/C (E-TEK) catalysts. More importantly, the advanced characterization technique X-ray absorption near edge structures (XANES) indicated a direct and solid evidence of the existence of strong interactions between ALD-Pt NPs and ZrC enabled by ALD. The results of this work provide insights for future design of electrocatalysts with high stability through increased interactions between catalyst particle and support.

The inherently sluggish kinetics of the oxygen reduction reaction (ORR) and instability of platinum (Pt) at the cathode are the big challenges for widespread commercialization of proton exchange membrane fuel cells, which are promising for portable, transportation, and stationary energy applications.[1–6] Currently, carbon black is the most widely used support material to promote Pt activity towards ORR. However, carbon black suffers corrosion during long-term fuel cell operation (especially at potential above 0.9 V) which results in the agglomeration of Pt nanoparticles (NPs) and thereby rapid degradation of Pt performance.[7–9] Furthermore, the weak interactions between carbon black and Pt NPs lead to sintering of the catalytic Pt NPs and a consequent decrease in the activity.[10,11] Besides the challenges to improve catalyst stabilities, it is highly desirable to improve Pt activity and decrease Pt loading in fuel cells because of the high cost and limited availability of Pt.[12–14] Therefore, it is extremely desirable to develop highly active and stable ORR electrocatalysts.

The challenges associated with using carbon black can be alleviated by substituting more corrosion-resistant support materials that have the strong metal–support interactions (SMSIs) with Pt.[15] The important role of SMSIs has been extensively studied for catalysis[16,17] where they not only improve the activity but also enhance the stability of catalysts.[18–20] More importantly, the effect of SMSIs for supported catalysts is mainly assumed to the result from the metal–support interface.[16,21]

There remains a challenge to further improve SMSIs particularly because it is difficult to precisely control the metal–support interface using conventional chemical methods. Atomic layer

[a] *Department of Mechanical and Materials Engineering, University of Western Ontario, London, ON N6A 5B9, Canada. E-mail: xsun@eng.uwo.ca*
[b] *State Key Laboratory of Advanced Technology for Materials Synthesis and Processing, Wuhan University of Technology, Wuhan 430070, People's Republic of China*
[c] *Department of Chemistry, University of Western Ontario, London, Ontario N6A 5B7, Canada*

† Electronic supplementary information (ESI) available: Experimental methods and supplementary data. See DOI: 10.1039/c4ee04086d

deposition (ALD) technique is a promising technique for precisely controlling the metal–support interface. ALD proceeds by forming chemical bonds between the initial layer of atoms of a reactive species and the surface of support during its first cycle, ensuring a strong interaction between the deposited material and support.[22–24] Electrical and interfacial properties of metal–support fabricated by ALD has been investigated.[25–28] ALD also has been carried out to prepare supported nobel metal NPs by employing sequential and self-limiting surface reactions.[24,29–31] Zirconium carbide (ZrC) is a very hard and conducting ceramic material with good corrosion resistance, high melting point, high stability, and good thermal conductivity. ZrC showed significantly stronger electrochemical corrosion resistance than Vulcan XC-72 (carbon black) support.[32,33] ZrC was found that it promoted the Pt ORR activity.[34] In this paper, we use ALD to enhance SMSIs through precisely controlling the metal–support interface at the atomic level. More corrosion-resistant Zirconium carbide (ZrC) was used as the support for deposition of ALD Pt. The ORR activity and durability of ALD deposited Pt on ZrC (ALD-Pt/ZrC) nanocomposites were explored and the nanocomposite showed greatly enhanced ORR activity and durability, compared with Pt/ZrC nanocomposites synthesized by a conventional chemical reduction method (denoted as CW-Pt/ZrC) and commercial Pt/C catalysts.

We first studied the electrochemical stability of the ZrC support relative to carbon black in acid solution. There are visible current peaks in the redox region for carbon black after oxidation treatment for 48 h (Fig. S1b†). These peaks indicate the surface oxide formation due to the hydroquinone–quinone (HQ–Q) redox couple on the carbon black surface. In contrast, ZrC has almost no change in the redox region. The electrochemical stability measurement confirms that ZrC is more resistant to electrochemical oxidation than carbon black (Fig. S1a†), consistent with previous results.[33] Support materials with higher oxidation resistance can hinder Pt NPs agglomeration caused by corrosion of the support, resulting in enhanced durability of the Pt catalyst.[35,36] The morphology of ALD-Pt/ZrC is shown in Fig. 1. Transmission electron microscopy (TEM) images clearly reveal that uniform Pt NPs are homogenously distributed on the ZrC support. The size of Pt NPs on ZrC is around 2–4 nm with narrow size distribution and the average size of Pt NPs is 3.2 nm in diameter, which is close to that of Pt NPs (3.4 nm) of CW-Pt/ZrC prepared from conventional chemical reduction method (Fig. S2†). The formation of ALD-Pt nanoparticles instead of continuous film are attributed to the following reasons: the limited appropriate surface nucleation site (functional groups) of the surface of ZrC for the reaction with Pt ALD reactants,[22] the difference of surface energy between Pt and substrates[37] and the natural tendency of noble metal atoms to diffuse and agglomerate.[38] Interestingly, ALD-Pt NPs are hemispherical shape of the particles (marked with cycles) instead of spherical shape formed in CW-Pt/ZrC. Similar hemispherical particles were observed in the other ceramic-supported precious metal catalysts.[39,40] Furthermore, ALD-Pt NPs bonded directly to the ZrC without any transition layers. We also found the lattice array of Pt {111} matches that of the ZrC {111} support (see the inset in Fig. 1b). This interfacial morphology suggests that the chemical interactions between Pt and ZrC is unusually strong.[41,42] The Pt loading for ALD-Pt/ZrC and CW-Pt/ZrC catalysts are determined to be 19 wt% and 23 wt% respectively by inductively coupled plasma-optical emission spectroscopy (ICP-OES).

X-ray absorption spectroscopy was used to identify the properties of Pt/ZrC catalysts prepared by different synthesis methods. Fig. 2 shows X-ray absorption near edge structures (XANES) spectra for both Pt L_3 and L_2 edge of ZrC supported Pt NPs. Pt foil is also analyzed for comparison. The whiteline (WL) in Pt L_2 and L_3 edges arises from the dominant $2p_{1/2}$ and $2p_{3/2}$ transition to $5d_{3/2}$ and $5d_{5/2,3/2}$, respectively (dipole selection rule: $\Delta l = \pm 1$, $\Delta j = \pm 1, 0$), indicating the presence of unoccupied densities of states of Pt $5d_{5/2}$ and $5d_{3/2}$ character in the samples.[43,44] There are no significant changes in the threshold energy (E_0) and the maximum energy (E_{peak}) of the Pt L_3 edge for the Pt/ZrC catalysts compared to the Pt foil, indicating the metallic nature of the deposited Pt catalysts (Fig. 2a). The intensity of Pt L_3 WL shows differences between the samples. The intensity of Pt L_3 WL is a qualitative indicator of electron vacancies in the 5d orbitals of Pt atoms. The change in the WL intensity at Pt L_3-edge of different samples is as follows: Pt foil < ALD-Pt/ZrC < CW-Pt/ZrC. The corresponding L_2 edge WL (Fig. 2b) showed a similar trend as that of the Pt L_3 edge in E_{peak} and E_0. The change in Pt L_2 WL intensity of the samples is

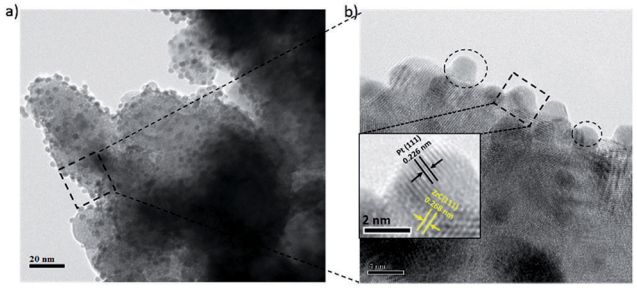

Fig. 1 TEM images of the ALD-Pt/ZrC catalyst: (a) low-magnification TEM of ALD-Pt/ZrC, (b) high-magnification TEM of ALD-Pt/ZrC.

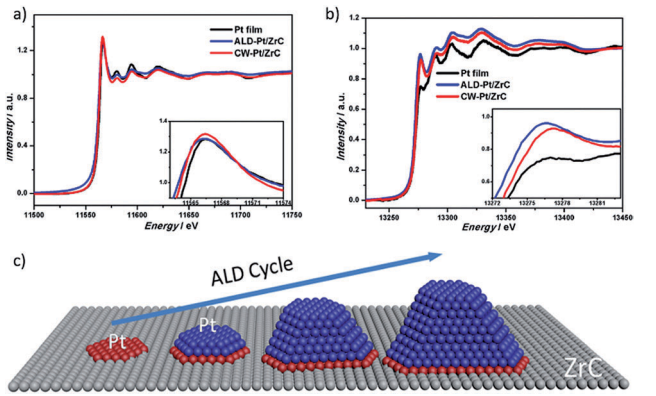

Fig. 2 Normalized XANES spectra of Pt nanoparticles on composite catalyst support at (a) the Pt L_3 edge and (b) the Pt L_2 edge. (c) Schematic illustration of ALD-Pt growth on ZrC support.

as follows: Pt foil < CW-Pt/ZrC < ALD-Pt/ZrC. According to the literature,[43,45,46] the changes in the WL intensity could be caused by size effects and/or electronic effects. The particle sizes of ALD-Pt/ZrC and CW-Pt/ZrC were similar; thus, the changes in the WL intensity for these catalyst samples are primarily a manifestation of electronic effects that induce changes in the d-band vacancy of Pt.[47] In order to understand the effect of the unoccupied densities of 5d states of Pt NPs on ZrC by different synthesis methods, quantitative WL analysis has been conducted as listed in Table 1 on the basis of a reported method[43,44,48] (see details in ESI†). These results indicated that ALD-Pt/ZrC catalyst has higher total unoccupied density of states of Pt 5d character compared with CW-Pt/ZrC, indicating that the interactions between Pt and ZrC support by ALD is higher than that of CW-Pt/ZrC prepared from conventional chemical reduction method. This important difference in SMSIs is attributed to the different synthesis mechanism of Pt NPs. ALD is a thin film deposition technique based on sequential and self-limiting surface reactions.[24,29,49–51] As shown in Fig. 2c, the Pt precursor ($MeCpPtMe_3$) was first deposited on the surface of ZrC and there is the very strong chemical interaction between Pt precursor and ZrC.[24,52] The first layer of Pt atoms is embedded into the ZrC support due to the high temperature (250 °C). With additional cycling, Pt clusters begin to form on the first layer of embedded Pt atoms, finally leading to growth of Pt NPs on the surface of ZrC. The shape of the metal NPs is usually controlled by the interfacial free energy and the surface free energy of the support.[53] Therefore, there are strong interactions between ALD-Pt hemispherical particles and the ZrC support at the embedded Pt–ZrC interfaces,[54] as evidenced by the combined results of HRTEM and XANES. For CW-Pt/ZrC catalyst, synthesized by conventional chemical reduction method, the spherical shape of the Pt NPs first forms in solution and then they are deposited on the surface of ZrC support, mainly through physical adsorption. This results in weak interactions between Pt and the ZrC support. Using ALD to grow the Pt nanoparticles holds an advantage over conventional wet chemical reduction as it can improve the interactions between metal and support through precise control of the metal–support interface at atomic level.

ORR measurements were performed in O_2-saturated 0.5 M H_2SO_4 electrolyte using a thin film catalyst deposited onto a glassy carbon rotating-disk electrode (RDE). Fig. S3† showed sufficient electronic conductivity was ensured by adding 20 wt% VulcanXC72R to the ZrC supported Pt catalysts to prepare the ink as previous study.[55] RDE experiments were performed to reveal the ORR kinetics of ALD-Pt/ZrC and CW-Pt/ZrC nanocomposites in comparison with the benchmark commercial Pt on carbon black catalyst (Pt/C) (Fig. 3). The half wave potential ($E_{1/2}$) of each catalyst was estimated by determining the maxima of the derivatives of the reduction current. ALD-Pt/ZrC nanocomposites is the most active catalyst, yielding the highest $E_{1/2}$ value of 0.858 V, which is higher than CW-Pt/ZrC nanocomposites ($E_{1/2}$: 0.839 V), and Pt/C ($E_{1/2}$: 0.818 V). It is obvious that ALD-Pt/ZrC nanocomposites have better electrocatalytic activity toward ORR than CW-Pt/ZrC nanocomposites and Pt/C catalysts. The ORR mass activity (based on Pt loading) and specific activity (based on electrochemical surface area (ECSA); see details in ESI†) of the tested catalysts are calculated and shown in Fig. 3b. The ORR specific activity of different nanocomposites increases in the order ALD-Pt/ZrC > CW-Pt/ZrC > Pt/C at the potential of 0.90 V. The higher ORR activity of ALD Pt/ZrC nanocomposites compared to CW-Pt/ZrC and Pt/C can be related to many factors, including geometric[56] and electronic effects.[57–59] The structure and particle size of Pt nanoparticles in all electrocatalysts are relatively similar. Thus, it is likely that the ORR enhancement of ALD Pt/ZrC nanocomposites is due to the change in the electronic structure of Pt nanoparticles deposited on ZrC using ALD. This is an indication of stronger metal support interaction between ALD Pt and ZrC support compared to CW-Pt. The surfaces with the best ORR activities should have an intermediate oxygen binding energy. Too weak oxygen binding energies impede O–O bond cleavage, while too strong binding energies that are inhibit the formation of O–H bonds and instead facilitate H_2O_2 formation.[60] The changes in the electronic structure of ALD-Pt facilitate the transition of the adsorbed OH to water by the modification of the binding energy of the oxygen-containing species.[61] The ALD-Pt/ZrC nanocomposites exhibited a specific activity of 0.23 mA cm^{-2} at 0.9 V, which was 2.8 times greater than that of Pt/C (0.08 mA cm^{-2}).

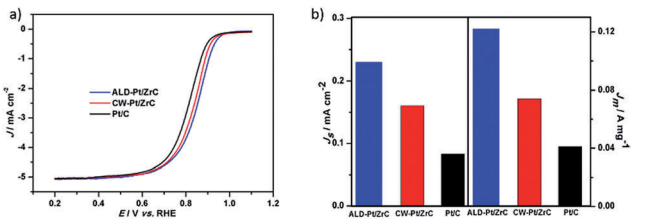

Fig. 3 (a) ORR curves of electrodes made from ALD-Pt/ZrC nanocomposites, CW-Pt/ZrC nanocomposites and E-TEK Pt/C catalysts in an O_2-saturated 0.5 M H_2SO_4 solution at room temperature (1600 rpm, sweep rate: 10 mV s^{-1}). (b) Specific activity and mass activity at 0.9 V (*vs.* RHE) for ALD-Pt/ZrC nanocomposites, CW-Pt/ZrC nanocomposites and E-TEK Pt/C catalysts.

Table 1 Summarizes the Pt L_3 and Pt L_2 edge threshold and WL parameters

	Pt L_3 edge WL				Pt L_2 edge WL					
Samples	E_0 (eV)	$E_{(peak)}$ (eV)	Γ (eV)	ΔA_3	E_0 (eV)	$E_{(peak)}$ (eV)	Γ (eV)	ΔA_3	$h_{5/2}$	$h_{3/2}$
Pt foil	11 564	11 566.4	4.4	6.8	13 273	13 277	2.2	2.27	0.634211	0.105553
ALD-Pt/ZrC	11 564	11 566.4	5.5	6.87	13 273	13 276.8	3.9	4.89	0.620616	0.227381
CW-Pt/ZrC	11 564	11 566.4	5.1	6.89	13 272.9	13 277.1	4.4	3.63	0.632293	0.168792

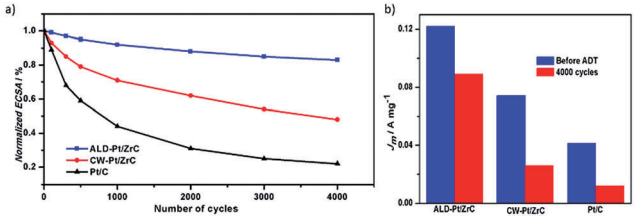

Fig. 4 (a) Loss of electrochemical surface area (ECSA) of ALD-Pt/ZrC nanocomposites, CW-Pt/ZrC nanocomposites and E-TEK Pt/C catalysts as a function of cycling numbers. (b) Mass activity at 0.9 V (*vs.* RHE) for ALD-Pt/ZrC nanocomposites, CW-Pt/ZrC nanocomposites and E-TEK Pt/C catalysts before and after ADT.

After normalized to the loading amount of Pt metal, the mass activity of ALD-Pt/ZrC nanocomposites was found to be 0.12 A mg_{Pt}^{-1}, which was 3.0 times greater than that of Pt/C (0.04 A mg_{Pt}^{-1}) (Fig. 3b).

Besides high catalytic activity, the ALD-Pt/ZrC nanocomposites showed remarkable catalytic stability. Accelerated durability tests (ADT) of the catalysts were conducted by potential cycling between 0.6 and 1.2 V *vs.* RHE at a scan rate of 50 mV s^{-1}. The Pt ECSA values of catalysts after potential cycling were calculated from their CVs (Fig. S4–S6†) and the normalized ECSA was plotted as a function of the cycle number (Fig. 4a). After 4000 cycles, the ALD-Pt/ZrC nanocomposites lost only 17% of its initial ECSA, whereas the Pt ECSA of the CW-Pt/ZrC nanocomposites and Pt/C decreased by 52% and 78% respectively. This finding demonstrated that the ALD-Pt/ZrC nanocomposites were almost 5-fold more stable than Pt/C and more than 3-fold more stable than CW-Pt/ZrC nanocomposites. ALD-Pt/ZrC catalyst also show higher stability compared with other reported ceramic supported catalysts as shown in Fig. S7.† The ORR activities after ADT test were also measured for all catalysts in O_2-staturated H_2SO_4 electrolyte. The polarization curves of CW-Pt/ZrC (Fig. S5b†) and Pt/C (Fig. S6b†) nanocomposites show more obvious current drop and more negative onset potentials after ADT, while there is less change for ALD-Pt/ZrC (Fig. S4b†). After ADT, the mass activity of ALD-Pt/ZrC nanocomposites at 0.9 V are 0.09 A mg^{-1}, while mass activities for CW-Pt/ZrC and Pt/C are 0.03 A mg^{-1} and 0.01 A mg^{-1}, respectively (Fig. 4b). The mass activity of ALD-Pt/ZrC nanocomposites after ADT is about 9 times higher than that of Pt/C.

The morphologies of the ALD-Pt/ZrC, CW-Pt/ZrC and Pt/C nanocomposites before and after ADT were examined by TEM. After the ADT test, the size of the Pt NPs in the Pt/C catalyst increased from 3–5 to 7–25 nm with a broad size distribution (Fig. S8†), indicating that serious ripening or aggregation of the Pt NPs occurred during the CV cycling. In contrast, after the ADT, the size of the Pt NPs in the ALD-Pt/ZrC nanocomposites increased from 3–5 to 3–7 nm with a narrow size distribution (Fig. 1 and S9†), suggesting that ALD-Pt/ZrC is more electrochemically stable than the Pt/C catalyst. The Pt NPs of CW-Pt/ZrC nanocomposites grow in size from 3–5 to 4–12 nm after the ADT as shown in Fig. S2,† consistent with the observed decrease in ECSA for this material.

The high activity of ALD-Pt/ZrC nanocomposites could be attributed to the synergetic effects between Pt and ZrC support such as the electronic structure change of Pt confirmed by results of XANES analysis, which may facilitate the catalysis of the ORR.[17] In general, the Pt ECSA decreases through (1) Ostwald ripening,[62] (2) coalescence of Pt NPs by Pt nanocrystal migration due to weak interactions of Pt NPs and support,[8,63] and (3) Pt NPs agglomeration caused by corrosion of the support material.[64,65] The greatly-enhanced ORR stability of the ALD-Pt/ZrC nanocomposites may arise from the excellent stability of the ZrC support and the SMSIs between the ALD-Pt NPs and the support that impede Pt migration. The results of the electrochemical tests showing enhanced ORR activity and durability can be well explained by the findings of the XANES analysis.

In summary, we have developed a robust Pt/ZrC catalyst by ALD that exhibits very high activity and durability towards ORR compared with Pt/ZrC prepared by conventional chemical reduction method and commercial Pt/C (E-TEK) catalysts. By using ALD to grow the Pt nanoparticles, we take advantage of the SMSIs at the atomic level between the Pt and ZrC, which are not present when NPs are deposited by conventional methods because of primarily physical adsorption at the surface. Our results suggest that ALD-Pt/ZrC catalysts show noticeable change in the electronic structure of Pt due to strong interactions with ZrC support enabled by ALD. ALD-Pt/ZrC nanocomposites show almost 5-fold more stable than Pt/C and more than 3-fold more stable than CW-Pt/ZrC nanocomposites. In a broader sense, this technique may prove extremely useful when complex synthesis and precise control of composite materials is needed. The results of this work provide a reliable way for future design of electro-catalysts with improved, strong interactions between metal NPs and the support materials.

Acknowledgements

This research was supported by Natural Sciences and Engineering Research Council of Canada (NSERC), Canada Research Chair (CRC) Program, Canada Foundation for Innovation (CFI), Ontario Research Fund (ORF), Canadian Light Source (CLS), McMaster National Microscopy Centre, and the University of Western Ontario.

Notes and references

1 Y. Bing, H. Liu, L. Zhang, D. Ghosh and J. Zhang, *Chem. Soc. Rev.*, 2010, **39**, 2184–2202.
2 J. Liang, Y. Jiao, M. Jaroniec and S. Z. Qiao, *Angew. Chem., Int. Ed.*, 2012, **51**, 11496–11500.
3 N. Cheng, H. Li, G. Li, H. Lv, S. Mu, X. Sun and M. Pan, *Chem. Commun.*, 2011, **47**, 12792–12794.
4 M. Shao, K. Shoemaker, A. Peles, K. Kaneko and L. Protsailo, *J. Am. Chem. Soc.*, 2010, **132**, 9253–9255.
5 I. E. L. Stephens, A. S. Bondarenko, U. Gronbjerg, J. Rossmeisl and I. Chorkendorff, *Energy Environ. Sci.*, 2012, **5**, 6744–6762.
6 Z. W. Chen, D. Higgins, A. P. Yu, L. Zhang and J. J. Zhang, *Energy Environ. Sci.*, 2011, **4**, 3167–3192.

7 N. Cheng, S. Mu, M. Pan and P. P. Edwards, *Electrochem. Commun.*, 2009, **11**, 1610–1614.
8 Z. Z. Jiang, Z. B. Wang, Y. Y. Chu, D. M. Gu and G. P. Yin, *Energy Environ. Sci.*, 2011, **4**, 728–735.
9 Z. Z. Jiang, Z. B. Wang, Y. Y. Chu, D. M. Gu and G. P. Yin, *Energy Environ. Sci.*, 2011, **4**, 2558–2566.
10 Y. Shao-Horn, W. C. Sheng, S. Chen, P. J. Ferreira, E. F. Holby and D. Morgan, *Top. Catal.*, 2007, **46**, 285–305.
11 N. Cheng, M. N. Banis, J. Liu, A. Riese, X. Li, R. Li, S. Ye, S. Knights and X. Sun, *Adv. Mater.*, 2015, **27**, 277–281.
12 J. Liang, R. F. Zhou, X. M. Chen, Y. H. Tang and S. Z. Qiao, *Adv. Mater.*, 2014, **26**, 6074–6079.
13 J. J. Duan, S. Chen, S. Dai and S. Z. Qiao, *Adv. Funct. Mater.*, 2014, **24**, 2072–2078.
14 R. F. Zhou and S. Z. Qiao, *Chem. Mater.*, 2014, **26**, 5868–5873.
15 Y. Y. Shao, G. P. Yin, Y. Z. Gao and P. F. Shi, *J. Electrochem. Soc.*, 2006, **153**, A1093–A1097.
16 M. Cargnello, V. V. T. Doan-Nguyen, T. R. Gordon, R. E. Diaz, E. A. Stach, R. J. Gorte, P. Fornasiero and C. B. Murray, *Science*, 2013, **341**, 771–773.
17 X. Han, F. Cheng, T. Zhang, J. Yang, Y. Hu and J. Chen, *Adv. Mater.*, 2014, **26**, 2047–2051.
18 R. Kou, Y. Shao, D. Mei, Z. Nie, D. Wang, C. Wang, V. V. Viswanathan, S. Park, I. A. Aksay, Y. Lin, Y. Wang and J. Liu, *J. Am. Chem. Soc.*, 2011, **133**, 2541–2547.
19 N. C. Cheng, J. Liu, M. N. Banis, D. S. Geng, R. Y. Li, S. Y. Ye, S. Knights and X. L. Sun, *Int. J. Hydrogen Energy*, 2014, **39**, 15967–15974.
20 Z. H. Zhang, J. Liu, J. J. Gu, L. Su and L. F. Cheng, *Energy Environ. Sci.*, 2014, **7**, 2535–2558.
21 T. Bunluesin, R. J. Gorte and G. W. Graham, *Appl. Catal., B*, 1998, **15**, 107–114.
22 K. Kim, H.-B.-R. Lee, R. W. Johnson, J. T. Tanskanen, N. Liu, M.-G. Kim, C. Pang, C. Ahn, S. F. Bent and Z. Bao, *Nat. Commun.*, 2014, **5**.
23 Y. Zhou, D. M. King, X. H. Liang, J. H. Li and A. W. Weimer, *Appl. Catal., B*, 2010, **101**, 54–60.
24 S. M. George, *Chem. Rev.*, 2010, **110**, 111–131.
25 C. Mukherjee, T. Das, C. Mahata, C. K. Maiti, C. K. Chia, S. Y. Chiam, D. Z. Chi and G. K. Dalapati, *ACS Appl. Mater. Interfaces*, 2014, **6**, 3263–3274.
26 D. Shahrjerdi, D. I. Garcia-Gutierrez, E. Tutuc and S. K. Banerjee, *Appl. Phys. Lett.*, 2008, **92**.
27 T. H. Hung, S. Krishnamoorthy, M. Esposto, D. N. Nath, P. S. Park and S. Rajan, *Appl. Phys. Lett.*, 2013, **102**.
28 M. N. Liu, X. L. Li, S. K. Karuturi, A. I. Y. Tok and H. J. Fan, *Nanoscale*, 2012, **4**, 1522–1528.
29 M. Knez, K. Niesch and L. Niinisto, *Adv. Mater.*, 2007, **19**, 3425–3438.
30 S. H. Sun, G. X. Zhang, N. Gauquelin, N. Chen, J. G. Zhou, S. L. Yang, W. F. Chen, X. B. Meng, D. S. Geng, M. N. Banis, R. Y. Li, S. Y. Ye, S. Knights, G. A. Botton, T. K. Sham and X. L. Sun, *Sci. Rep.*, 2013, **3**, 1775.
31 H. Feng, J. W. Elam, J. A. Libera, W. Setthapun and P. C. Stair, *Chem. Mater.*, 2010, **22**, 3133–3142.
32 Y. C. Kimmel, X. Xu, W. Yu, X. Yang and J. G. Chen, *ACS Catal.*, 2014, **4**, 1558–1562.
33 W. L. Qu, Z. B. Wang, X. L. Sui, D. M. Gu and G. P. Yin, *Fuel Cells*, 2013, **13**, 149–157.
34 P. Justin, P. H. K. Charan and G. R. Rao, *Appl. Catal., B*, 2014, **144**, 767–774.
35 Y. Liu and W. E. Mustain, *J. Am. Chem. Soc.*, 2013, **135**, 530–533.
36 H. F. Lv, S. C. Mu, N. C. Cheng and M. Pan, *Appl. Catal., B*, 2010, **100**, 190–196.
37 I. J. Hsu, D. A. Hansgen, B. E. McCandless, B. G. Willis and J. G. Chen, *J. Phys. Chem. C*, 2011, **115**, 3709–3715.
38 A. J. M. Mackus, M. A. Verheijen, N. Leick, A. A. Bol and W. M. M. Kessels, *Chem. Mater.*, 2013, **25**, 1905–1911.
39 M. Tsujimoto, S. Moriguchi, S. Isoda, T. Kobayashi and T. Komatsu, *J. Electron Microsc.*, 1999, **48**, 361–366.
40 S. Bernal, R. T. Baker, A. Burrows, J. J. Calvino, C. J. Kiely, C. Lopez-Cartes, J. A. Perez-Omil and J. M. Rodriguez-Izquierdo, *Surf. Interface Anal.*, 2000, **29**, 411–421.
41 N. Kamiuchi, T. Matsui, R. Kikuchi and K. Eguchi, *J. Phys. Chem. C*, 2007, **111**, 16470–16476.
42 X. Liu, M.-H. Liu, Y.-C. Luo, C.-Y. Mou, S. D. Lin, H. Cheng, J.-M. Chen, J.-F. Lee and T.-S. Lin, *J. Am. Chem. Soc.*, 2012, **134**, 10251–10258.
43 M. N. Banis, S. Sun, X. Meng, Y. Zhang, Z. Wang, R. Li, M. Cai, T.-K. Sham and X. Sun, *J. Phys. Chem. C*, 2013, **117**, 15457–15467.
44 T. K. Sham, S. J. Naftel and I. Coulthard, *J. Appl. Phys.*, 1996, **79**, 7134–7138.
45 J. G. Zhou, X. T. Zhou, X. H. Sun, R. Y. Li, M. Murphy, Z. F. Ding, X. L. Sun and T. K. Sham, *Chem. Phys. Lett.*, 2007, **437**, 229–232.
46 D.-Y. Wang, C.-H. Chen, H.-C. Yen, Y.-L. Lin, P.-Y. Huang, B.-J. Hwang and C.-C. Chen, *J. Am. Chem. Soc.*, 2007, **129**, 1538–1540.
47 V. T. T. Ho, C.-J. Pan, J. Rick, W.-N. Su and B.-J. Hwang, *J. Am. Chem. Soc.*, 2011, **133**, 11716–11724.
48 A. N. Mansour, J. W. Cook and D. E. Sayers, *J. Phys. Chem.*, 1984, **88**, 2330–2334.
49 J. W. Elam, N. P. Dasgupta and F. B. Prinz, *MRS Bull.*, 2011, **36**, 899–906.
50 C. Marichy, M. Bechelany and N. Pinna, *Adv. Mater.*, 2012, **24**, 1017–1032.
51 R. L. Puurunen, *J. Appl. Phys.*, 2005, **97**, 121301.
52 R. J. Narayan, S. P. Adiga, M. J. Pellin, L. A. Curtiss, A. J. Hryn, S. Stafslien, B. Chisholm, C. C. Shih, C. M. Shih, S. J. Lin, Y. Y. Su, C. M. Jin, J. P. Zhang, N. A. Monteiro-Riviere and J. W. Elam, *Philos. Trans. R. Soc., A*, 2010, **368**, 2033–2064.
53 J. A. Enterkin, K. R. Poeppelmeier and L. D. Marks, *Nano Lett.*, 2011, **11**, 993–997.
54 N. Ta, J. J. Liu, S. Chenna, P. A. Crozier, Y. Li, A. Chen and W. Shen, *J. Am. Chem. Soc.*, 2012, **134**, 20585–20588.
55 D. Wang, C. V. Subban, H. Wang, E. Rus, F. J. DiSalvo and H. D. Abruña, *J. Am. Chem. Soc.*, 2010, **132**, 10218–10220.
56 Y. Z. Wang, Y. M. Xie, P. R. Wei, H. F. Schaefer, P. V. Schleyer and G. H. Robinson, *J. Am. Chem. Soc.*, 2013, **135**, 19139–19142.
57 Y. H. Chung, D. Y. Chung, N. Jung and Y. E. Sung, *J. Phys. Chem. Lett.*, 2013, **4**, 1304–1309.

58 S. Mukerjee, S. Srinivasan, M. P. Soriaga and J. McBreen, *J. Electrochem. Soc.*, 1995, **142**, 1409–1422.
59 V. S. Murthi, R. C. Urian and S. Mukerjee, *J. Phys. Chem. B*, 2004, **108**, 11011–11023.
60 J. L. Zhang, M. B. Vukmirovic, Y. Xu, M. Mavrikakis and R. R. Adzic, *Angew. Chem., Int. Ed.*, 2005, **44**, 2132–2135.
61 S. J. Yoo, S. J. Hwang, J. G. Lee, S. C. Lee, T. H. Lim, Y. E. Sung, A. Wieckowski and S. K. Kim, *Energy Environ. Sci.*, 2012, **5**, 7521–7525.
62 P. J. Ferreira, G. J. la O', Y. Shao-Horn, D. Morgan, R. Makharia, S. Kocha and H. A. Gasteiger, *J. Electrochem. Soc.*, 2005, **152**, A2256–A2271.
63 B. Y. Xia, B. Wang, H. B. Wu, Z. Liu, X. Wang and X. W. Lou, *J. Mater. Chem.*, 2012, **22**, 16499–16505.
64 S. Y. Huang, P. Ganesan, S. Park and B. N. Popov, *J. Am. Chem. Soc.*, 2009, **131**, 13898–13899.
65 L. Zhang, L. Y. Wang, C. M. B. Holt, B. Zahiri, Z. Li, K. Malek, T. Navessin, M. H. Eikerling and D. Mitlin, *Energy Environ. Sci.*, 2012, **5**, 6156–6172.